

Settling and collision between small ice crystals in turbulent flows

Jennifer Jucha,¹ Aurore Naso,² Emmanuel Lévêque,² and Alain Pumir³

¹*Projekträger Jülich, Forschungszentrum Jülich GmbH, 52425 Jülich, Germany*

²*Laboratoire de Mécanique des Fluides et d'Acoustique, CNRS, École Centrale de Lyon, Université de Lyon, INSA de Lyon, 36 avenue Guy de Collongue, 69134 Écully Cedex, France*

³*Laboratoire de Physique, CNRS, École Normale Supérieure de Lyon, Université de Lyon, 46 allée d'Italie, 69364 Lyon Cedex 07, France*



(Received 10 May 2017; published 11 January 2018)

Ice crystals are present in a variety of clouds, at sufficiently low temperature. We consider here mixed-phase clouds which, at temperature $\gtrsim -20^\circ\text{C}$, contain ice crystals, shaped approximately as thin oblate ellipsoids. We investigate the motion of these particles transported by an isotropic turbulent flow and, in particular, the collision between these crystals, a key process in the formation of graupels. Using fully resolved direct numerical simulations, and neglecting the effects of fluid inertia on the particle motion, we determine the influence of the turbulence intensity and of gravitational settling, in a realistic range of parameters. At small turbulent energy dissipation rate, collisions are induced mainly by differential gravitational settling between particles with different orientations. The effect has a clear signature on the relative orientation of colliding ellipsoids. As the turbulent energy dissipation rate increases, however, the influence of the turbulent velocity fluctuations becomes the dominant effect determining the collision rate. Using simple estimates, we propose an elementary understanding of the relative importance of gravitational settling and turbulent fluctuations.

DOI: [10.1103/PhysRevFluids.3.014604](https://doi.org/10.1103/PhysRevFluids.3.014604)

I. INTRODUCTION

The condensation of water vapour in many types of clouds starts with very small liquid droplets and ice crystals [1]. Whereas much work has been devoted lately to the formation of rain drops in warm clouds, where the ice phase is totally absent [2–4], comparably much less work has been devoted to the aggregation of small crystals to form larger clusters. The aim of the present work is to investigate the effect of turbulence on the formation of graupels by aggregation of small crystals.

We are interested here in the class of “mixed-phased” clouds, where water vapor droplets coexist with ice crystals. This is typically the case in cumulus clouds, in a range of temperature T between $-30^\circ\text{C} \lesssim T \lesssim 0^\circ\text{C}$. The shape of the crystals depends on the temperature [1,5]. Over a range of temperatures ($-20^\circ\text{C} \lesssim T \lesssim -10^\circ\text{C}$), ice crystals are shaped like snowflakes (they are columnar shaped at lower temperature, or in the range $-10^\circ\text{C} \lesssim T \lesssim -5^\circ\text{C}$ [1,5,6]). We are focusing in this work on the class of crystals with an oblate shape.

It is known that gravitational settling plays a significant role in cloud microphysics processes involving ice crystals [1,7,8]. The anisotropic nature of the crystals results in an anisotropy of the drag coefficients [9] which implies a dependence of the settling velocity as a function of the orientation of the crystal in the fluid. Understanding precisely the distribution of orientation of crystals settling in a turbulent flow with respect to gravity, \mathbf{g} , is still a subject of active research [1,9–12]. This orientation distribution controls important properties of the clouds, including those related to light or radiation reflection [1,13,14]. A previous study, at relatively low turbulence intensity [15] has stressed the importance of the dispersion of the settling velocity in determining the collision rate

between crystals [15]; turbulence seemed to play a rather minor role. This is in sharp contrast with the problem of collision of droplets in turbulent warm clouds, where, in the absence of any differential gravitational settling, turbulence has been argued to play the major role in determining the collision kernel [16–20].

In this work, we determine the collision rate of crystals in a turbulent flow, at different turbulence intensity, measured by the energy dissipation rate, ε , chosen in the range $1 \text{ cm}^2/\text{s}^3 \lesssim \varepsilon \lesssim 256 \text{ cm}^2/\text{s}^3$. We perform direct numerical simulations of homogeneous, isotropic turbulent flows, using a simplified model of ice crystal dynamics [10,21,22]. To disentangle the relative roles of turbulence and gravity, we determine the collision rates both with and without gravity. Whereas our results, in full agreement with Ref. [15], point to a dominant role of differential settling at low turbulence intensity, they indicate that turbulence plays a much more prominent role at higher intensity. This is due, in particular, to the strong effect of the inertial effects in the motion of particles, qualitatively consistent with what has been found in the problem of collision between droplets in warm clouds [18–20].

We begin by reviewing the simplifying assumptions used to study the problem, along with the underlying equations and the numerical methods used; see Sec. II. We then study in Sec. III the statistics of orientation and of settling of the ellipsoids. The collisions statistics of these objects are presented and discussed in Sec. IV. Concluding remarks are finally given in Sec. V.

II. SETTING UP THE PROBLEM

Turbulent flows in clouds occur at a very high Reynolds number and are influenced by many factors, including buoyancy. In addition, the shapes of ice crystals are rather complicated. A fully realistic numerical study of the problem appears impossible, and, for this reason, a number of simplifying assumptions have been introduced. In the following, we summarize these approximations and present the resulting equations of motion, as well as the numerical methods used.

A. Turbulent flow

1. Simplifying assumptions

Homogeneous and isotropic turbulence is used as a paradigm for the motion of the carrier fluid. A turbulent flow is simulated by direct numerical simulation (DNS) in a periodic box of size $8\pi \text{ cm} \approx 25 \text{ cm}$, which represents a subdomain of the cloud. In this box, turbulence is sustained at large scales by an external forcing with an energy injection rate ε (per unit mass) equal to $\varepsilon = 0.976 \text{ cm}^2/\text{s}^3$, $15.62 \text{ cm}^2/\text{s}^3$, and $246.4 \text{ cm}^2/\text{s}^3$. The choice of a realistic value of the fluid viscosity, $\nu \approx 0.1132 \text{ cm}^2/\text{s}$, ensures that in our simulations, the smallest length and time scales of the flows match those in the cloud. Namely, the size of the smallest eddies in the flow, the Kolmogorov length scale is $\eta \equiv (\nu^3/\varepsilon)^{1/4}$, and the fastest time scale, τ_K , is $\tau_K \equiv (\nu/\varepsilon)^{1/2}$.

The small size of our computational system strongly limits the Reynolds numbers in the simulations. The intensity of turbulence is often characterized by the Reynolds number based on the Taylor microscale, Re_λ . It is defined as $\text{Re}_\lambda = u_{\text{rms}}\lambda/\nu$, where $\lambda = \sqrt{15}u_{\text{rms}}^2\nu/\varepsilon$ and $u_{\text{rms}}^2 = \langle u_x^2 \rangle$ (u_x is the x component of the fluid velocity, which by isotropy is equivalent to any other component in the flow). In our setup, with a fixed system size and viscosity, the relation between Re_λ and ε is one-to-one. In our simulations, Re_λ takes the values $\text{Re}_\lambda \approx 56$ ($\varepsilon = 0.976 \text{ cm}^2/\text{s}^3$), $\text{Re}_\lambda \approx 95$ ($\varepsilon = 15.62 \text{ cm}^2/\text{s}^3$), and $\text{Re}_\lambda \approx 151$ ($\varepsilon = 246.4 \text{ cm}^2/\text{s}^3$), which are much smaller than in clouds. In a system with a given size and a fixed viscosity, the Reynolds number Re_λ grows essentially as $\text{Re}_\lambda \propto \varepsilon^{1/6}$. As has been documented many times, the fluctuations of the velocity gradient become more extreme when the Reynolds number increases [23]. For this reason, our turbulent flow could conceivably underestimate the role of turbulence.

We would like to stress that our choice of a simplified turbulent flow potentially leaves aside important aspects of the flow in a cloud. It nonetheless allows us to obtain accurate numerical data and to improve our understanding of the various physical effects affecting the collision rate.

2. Numerical methods

In practice, the Navier-Stokes equations are solved:

$$\partial_t \mathbf{u} + (\mathbf{u} \cdot \nabla) \mathbf{u} = -\frac{\nabla p}{\rho_f} + \nu \nabla^2 \mathbf{u} + \mathbf{f}, \quad (1)$$

$$\nabla \cdot \mathbf{u} = 0, \quad (2)$$

where \mathbf{u} and p , respectively, denote the velocity and pressure fields, ν is the kinematic viscosity of the fluid, and ρ_f is its mass density. These equations are solved by using a pseudospectral method in a triply periodic domain. The flow is maintained statistically stationary by stirring the velocity field with a force (per unit mass), \mathbf{f} , acting on low wave numbers and such that the injected power ($\mathbf{f} \cdot \mathbf{u}$), averaged over the entire volume, remains constant and equal to ε . The solution is fully dealiased by using the 2/3 rule [24]. Specifically, if N is the number of grid points in each direction, the nonlinear term is computed by using only Fourier modes $0 \leq n \leq N/3$. The number of points taken here are $N = 384, 768$, and 1536 . The energy dissipation rate ε has been adjusted so that $k_{\max} \eta \gtrsim \pi$, η being the characteristic size of the smallest eddies, known as the Kolmogorov scale $\eta = (\nu^3/\varepsilon)^{1/4}$, and $k_{\max} = N/3$ being the highest wave number represented. With our resolution, the velocity gradients can be faithfully interpolated at the position of the ellipsoids. The numerical integration rests on a second-order accurate in time Runge-Kutta scheme.

B. Ice crystals dynamics

1. Simplifying assumptions

As a simplified assumption, the snowflake-shaped ice crystals are approximated here as very thin oblate ellipsoids of revolution (a spheroid), with a very small aspect ratio β between the short and the long axes, $\beta = c/a \sim 0.01$. We chose a realistic value for the long axis of the particles, $a = 150 \mu\text{m}$. Most of the calculations were carried out with the value of $\beta = 0.02$. We investigated the role of the shape of the ellipsoid by varying β at the intermediate value of $\varepsilon \approx 16 \text{ cm}^2/\text{s}^3$ ($\beta = 0.01$ and $\beta = 0.05$). The equations describing the motion of the very small ellipsoids are obtained by neglecting all effects of inertia of the fluid, that is, by using the assumption that the local Reynolds number is very small, so the Stokes equations can be used [21,22].

Our approach relies on a *one-way coupling* approach, which ignores the feedback induced by the motion of the particles on the fluid motion. This approximation is well justified when the particle volume fraction is very low [25].

2. Equations of motion

The equations of motion of the ellipsoids are derived by using the expressions of the force and of the torque acting on them by neglecting fluid inertia, that is, by assuming the Reynolds number based on the difference between the velocity of the fluid, \mathbf{u} , and that of the particle, \mathbf{v} , to be very small. Specifically, by solving the hydrodynamics in the low Reynolds number limit, the equation for the translational motion of the center of mass of the ellipsoids reduces to [22]

$$\frac{d\mathbf{v}}{dt} = \mathbf{g} + \frac{\nu\rho_f}{m_c} \mathbf{R}^{-1} \hat{\mathbf{K}} \mathbf{R} \cdot (\mathbf{u} - \mathbf{v}), \quad (3)$$

where $m_c = 4\rho_p\pi a^3\beta/3$ is the mass of the crystal (ρ_p is the particle density). In Eq. (3), \mathbf{R} is the rotation matrix between the laboratory coordinate system, (x, y, z) , and a particle fixed reference system, $(\hat{x}, \hat{y}, \hat{z})$, chosen in such a way that \hat{x} and \hat{y} correspond to the elongated directions of the ellipsoid, and \hat{z} to its short direction. In this frame, the resistance tensor $\hat{\mathbf{K}}$ has a simple diagonal form:

$$\hat{\mathbf{K}} = 16\pi a^3 \beta \text{diag}(1/(\chi_0 + a^2\alpha_0), 1/(\chi_0 + a^2\alpha_0), 1/(\chi_0 + a^2\beta^2\gamma_0)). \quad (4)$$

The values of the coefficients are $\alpha_0 = [\beta^2/(\beta^2 - 1) + \arccos(\beta)\beta/(1 - \beta^2)^{3/2}]$, $\gamma_0 = [-2/(\beta^2 - 1) - 2 \arccos(\beta)\beta/(1 - \beta^2)^{3/2}]$, and $\chi_0 = [2a^2\beta \arccos(\beta)/\sqrt{1 - \beta^2}]$.

As the ellipsoids are subject to a torque by the action of the fluid [21], they rotate with an angular velocity $\boldsymbol{\Omega} \equiv (\Omega_x, \Omega_y, \Omega_z)$ in the frame of reference attached to the ellipsoid (as mentioned above). The equation of motion for $\boldsymbol{\Omega}$ is obtained by equating the rate of change of angular momentum with torque:

$$\frac{d}{dt} \begin{pmatrix} \Omega_x \\ \Omega_y \\ \Omega_z \end{pmatrix} = \begin{pmatrix} \Omega_y \Omega_z \frac{\beta^2 - 1}{1 + \beta^2} \\ \Omega_z \Omega_x \frac{1 - \beta^2}{1 + \beta^2} \\ 0 \end{pmatrix} + 20 \frac{\rho_f}{\rho_p} \frac{v}{a^2} \begin{pmatrix} \frac{1}{\alpha_0 + \beta^2 \gamma_0} & 0 & 0 \\ 0 & \frac{1}{\alpha_0 + \beta^2 \gamma_0} & 0 \\ 0 & 0 & \frac{1}{2\alpha_0} \end{pmatrix} \begin{pmatrix} \frac{1 - \beta^2}{1 + \beta^2} \hat{\mathbf{S}}_{yz} + (\hat{\Omega}_{zy} - \Omega_x) \\ \frac{\beta^2 - 1}{1 + \beta^2} \hat{\mathbf{S}}_{xz} + (\hat{\Omega}_{xz} - \Omega_y) \\ (\hat{\Omega}_{yx} - \Omega_z) \end{pmatrix}, \quad (5)$$

where $\hat{\mathbf{S}}$ and $\hat{\boldsymbol{\Omega}}$ are the rate of strain and rate of rotation tensors in the reference frame of the ellipsoid, respectively defined as the symmetric and antisymmetric parts of the velocity gradient tensor in the same frame, $\hat{\mathbf{A}} = \mathbf{R}\mathbf{A}\mathbf{R}^{-1}$ ($A_{ij} = \partial_j u_i$): $\hat{\mathbf{S}} = (\hat{\mathbf{A}} + \hat{\mathbf{A}}^t)/2$, $\hat{\boldsymbol{\Omega}} = (\hat{\mathbf{A}} - \hat{\mathbf{A}}^t)/2$. The rate of rotation of the reference frame, $\boldsymbol{\Omega}$, allows us to determine the rotation matrix \mathbf{R} from the ellipsoid coordinate system to the laboratory frame.

The equations of motion (3) and (5) have been implemented in the code, and the numerical results have been carefully compared with those obtained, in the case of simple flows, using Mathematica. In particular, we used a still flow ($\mathbf{u} = \mathbf{0}$) or elementary flows with a few Fourier series modes; on all these flows, we made sure that the solutions were identical to machine accuracy.

3. Equations of motion in the limiting case of very thin ellipsoids

As we are interested here mainly in very small values of β , the resistance tensor $\hat{\mathbf{K}}$ in Eq. (4) reduces to $\hat{\mathbf{K}} \approx 32a \text{diag}(1/3, 1/3, 1/2)$. As a consequence, the equation of motion (3) can be simply expressed in terms of the response time τ_{Sp} of a sphere of radius a in the flow:

$$\frac{d\mathbf{v}}{dt} = \mathbf{g} + \frac{16}{3\pi\beta\tau_{Sp}} \mathbf{R}^{-1} \begin{pmatrix} 1/3 & 0 & 0 \\ 0 & 1/3 & 0 \\ 0 & 0 & 1/2 \end{pmatrix} \mathbf{R} \cdot (\mathbf{u} - \mathbf{v}), \quad (6)$$

where

$$\tau_{Sp} = \frac{2a^2}{9\nu} \frac{\rho_p}{\rho_f}. \quad (7)$$

From Eq. (6), the characteristic time of the translational dynamics is of the order of $\beta\tau_{Sp}$. Similarly, the expressions $\alpha_0 \approx \pi\beta/2$ and $\gamma_0 \approx 2$, valid when $\beta \rightarrow 0$ reduce the matrix $\text{diag}(1/(\alpha_0 + \beta^2\gamma_0), 1/(\alpha_0 + \beta^2\gamma_0), 1/(2\alpha_0))$ in Eq. (5) to $\frac{2}{\pi\beta} \text{diag}(1, 1, 1/2)$. This implies that the characteristic time scale of the evolution of $\boldsymbol{\Omega}$ is $\sim \beta\tau_{Sp}$.

4. Equations of motion: Dimensionless numbers

In the case of spherical particles, it is customary to compare the effects of turbulence, gravitational settling, and particle inertia by introducing dimensionless numbers. Namely, the particle relaxation time can be inferred from (6) to be $\tau_p \approx 2\beta\tau_{Sp}$. Comparing this time scale to the Kolmogorov time scale leads naturally to the definition of the Stokes number:

$$\text{St} \equiv 2\beta \frac{\tau_{Sp}}{\tau_K}. \quad (8)$$

To characterize the relative importance of gravitational settling and turbulence, we introduce the dimensionless gravity parameter, $S_{v,s}$, defined as the ratio between the settling velocity, of order $g\tau_p$,

and the velocity differences at the Kolmogorov scale, $(\varepsilon\nu)^{1/4}$ [26]. Using (6), we introduce

$$S_{v,s} \equiv 2\beta \frac{g\tau_{Sp}}{(\nu\varepsilon)^{1/4}}. \quad (9)$$

Recent work [12] demonstrates that the distribution of orientation depends on the Stokes number and on $S_{v,L} = S_{v,s}/Re_\lambda^{1/2}$. In turbulent flows, the ratio between the root-mean-square (rms) velocity, $\langle u_x^2 \rangle^{1/2}$ and the velocity scale at the Kolmogorov scale, $(\nu\varepsilon)^{1/4}$, is $\propto Re_\lambda^{1/2}$, which indicates that the settling velocity $g\tau_{Sp}$ should be compared with $\langle u_x^2 \rangle^{1/2}$. This leads us to introduce the gravity parameter $S_{v,L}$, based on the large-scale velocity of the flow:

$$S_{v,L} \equiv 2\beta \frac{g\tau_{Sp}}{\langle u^2 \rangle^{1/2}}. \quad (10)$$

In our study, the ratio between $S_{v,L}$ and $S_{v,s}$ is $\propto \varepsilon^{-1/12}$ or, equivalently, $\propto Re_\lambda^{-1/2}$.

C. Collisions

1. Simplifying assumptions

We focus in this study on the geometrical collision rate [4,27] by neglecting any hydrodynamic interactions occurring when particles are very close to each other [1,28], as well as molecular effects [29] which play a crucial role during the coagulation process. We also use the ‘‘ghost-collision’’ approximation [17,30,31], which consists in simulating a large number of trajectories in the flow, and in simply determining when two particles touch each other. This approximation has been used in many studies and has been thoroughly tested in the case of spherical particles [31].

2. Algorithm for collision detection

Collision detection between particles of nonspherical shapes requires a special approach. We follow here the one proposed by Siewert and collaborators [32] and implemented in particular in Ref. [15]. The method of detection is based on the work of Choi *et al.* [33]. Specifically, for each ellipsoid, one expresses the equation of the surface in the form: $\mathbf{X} \cdot \mathbf{B}_i \cdot \mathbf{X} = 1$, where \mathbf{X} is a vector in four dimensions: $\mathbf{X} = (x, y, z, 1)$, and the matrix \mathbf{B}_i characterizes the i th ellipsoid. To detect possible contacts between ellipsoids i and j , one computes the fourth-order polynomial: $P_{ij}(\lambda) = \det(\mathbf{B}_i - \lambda\mathbf{B}_j)$. It is known [33] that the polynomial P_{ij} has exactly two positive, real roots. Whether the two ellipsoids i and j are in contact can be determined from the nature of the two other roots of P_{ij} , that can be real (negative) or complex. In the former case, the two ellipsoids are separated, in the latter they overlap. When they are in contact, the polynomial P_{ij} has a real, negative double root. The algorithm implemented for collision detection consists in representing, for each pair of ellipsoids, the evolution of the polynomial P_{ij} as a function both of λ and of t , and in detecting the formation of a negative double root of P_{ij} .

3. Practical implementation of the collision detection algorithm

We followed a set of $N_{\text{ell}} = 70^3$ (respectively $N_{\text{ell}} = 100^3$) ellipsoids in a turbulent flow in the presence (respectively absence) of gravitational settling. Before processing the ellipsoids for collision detection, we let them equilibrate in the flow for at least $50\tau_K$, where $\tau_K \equiv (\nu/\varepsilon)^{1/2}$ is the Kolmogorov time. In all our runs, this long equilibration time is at least 100 times larger than the particle relaxation time. We subsequently followed the motion of the ellipsoids for at least $170\tau_K$, or equivalently, 14 times T_L , the integral (or correlation) time scale of the velocity field.

To check the quality of the statistics, and in particular the lack of any unstationary effects, we divided the runs into shorter ones, with time intervals of length $\approx 25\tau_K$, and determined the various averages, particularly the collision rates based on these shorter runs. The collision rates determined from these differed by less than a few percent from the collision rates reported here. Overall, the statistics presented in Sec. IV were determined with at least 72 000 recorded collisions.

TABLE I. Values of the physical parameters used in the simulation. The fluid consists of moist air, whose volumic mass and viscosity are ρ_f and ν . The ice particles have a volumic mass ρ_p and a major axis a . The gravity magnitude is g .

| Fluid | | Particles | | Gravity |
|-------------------------------|----------------------------|-------------------------------|----------|--------------------------|
| ρ_f (g/cm ³) | ν (cm ² /s) | ρ_p (g/cm ³) | a (cm) | g (cm/s ²) |
| 1.413×10^{-3} | 0.1132 | 0.9194 | 0.015 | 981 |

D. Parameters

1. Physical parameters

To approach realistic conditions, we have fixed various physical constants in a range relevant to the dynamics of ice crystals in clouds, presented in Table I.

2. List of runs

Our results are based on several calculations, obtained at different values of ε , the rate of energy injected in the flow, and the aspect ratio β of the particles. The list of the runs is presented in Table II, from which several observations can be made.

The effect of the settling induces a systematic drift of the particles in the computational box. In this context, the use of periodic boundary conditions in the vertical direction may become problematic if the settling becomes very fast, so that heavy particles go through the periodicity box in a time which is shorter than the turbulence decorrelation time. Specifically, let U_{sett} be the average settling velocity ($U_{\text{sett}} = -\langle v_z \rangle$) and $T_{\text{sett}} \approx L/U_{\text{sett}}$ the characteristic time of settling of the particles through the entire box. Provided T_{sett} is large compared to the decorrelation time of the turbulent velocity field T_L , however, the particle is submitted to a velocity field that significantly differs from that at earlier time. We observe that the value of the settling velocity measured for $\beta = 0.05$ and $\varepsilon \approx 16 \text{ cm}^2/\text{s}^3$ is $U_{\text{sett}} \approx 23.44 \text{ cm/s}$, so particles settle in a time of $\approx 1 \text{ s}$ through the computational box $L \approx 25.1 \text{ cm}$. This time is larger than the decorrelation time of the velocity field by a factor ≈ 2 , which guarantees that the use of periodic boundary conditions in the vertical direction does not lead to spurious effects.

Table II shows that the Stokes number, defined by Eq. (8), varies from ≈ 0.03 at $\varepsilon \approx 1 \text{ cm}^2/\text{s}^3$, up to values ≈ 0.5 at $\varepsilon \approx 256 \text{ cm}^2/\text{s}^3$. We note that in the related problem of collisions between

TABLE II. Characteristics of the runs discussed here. T_L and τ_K , respectively, denote the integral and Kolmogorov time scales. T_{run} refers to the time over which collision statistics have been computed. The number of ellipsoids used to estimate the statistical properties is N_{ell} ; the rms of the turbulent velocity fluctuations is u_{rms} , and the settling velocity U_{sett} (in runs with **g**, i.e., with a “Y” in the “gravity” column).

| | ε (cm ² /s ³) | Re_λ | β | τ_K (s) | T_L (s) | T_{run} (s) | Gravity | N_{ell} | u_{rms} (cm/s) | U_{sett} (cm/s) | St | $S_{v,s}$ | $S_{v,L}$ |
|--------|--|---------------------|---------|--------------|-----------|----------------------|---------|------------------|-------------------------|--------------------------|-------|-----------|-----------|
| Run 1 | 0.976 | 55.8 | 0.02 | 0.341 | 1.96 | 59.6 | Y | 70^3 | 2.18 | 9.78 | 0.034 | 17.0 | 4.5 |
| Run 2 | 0.976 | 55.8 | 0.02 | 0.341 | 1.96 | 59.6 | N | 100^3 | 2.18 | 0 | 0.034 | 0 | 0 |
| Run 3 | 15.62 | 94.6 | 0.02 | 0.085 | 0.696 | 14.6 | Y | 100^3 | 5.72 | 9.60 | 0.135 | 8.3 | 1.7 |
| Run 4 | 15.62 | 94.6 | 0.02 | 0.085 | 0.696 | 14.9 | N | 100^3 | 5.72 | 0 | 0.135 | 0 | 0 |
| Run 5 | 15.62 | 94.6 | 0.01 | 0.085 | 0.696 | 14.6 | Y | 70^3 | 5.72 | 4.88 | 0.068 | 4.2 | 0.85 |
| Run 6 | 15.62 | 94.6 | 0.01 | 0.085 | 0.696 | 14.9 | N | 100^3 | 5.72 | 0 | 0.068 | 0 | 0 |
| Run 7 | 15.62 | 94.6 | 0.05 | 0.085 | 0.696 | 14.6 | Y | 70^3 | 5.72 | 23.44 | 0.34 | 20.3 | 4.1 |
| Run 8 | 15.62 | 94.6 | 0.05 | 0.085 | 0.696 | 14.9 | N | 100^3 | 5.72 | 0 | 0.34 | 0 | 0 |
| Run 9 | 246.4 | 151.2 | 0.02 | 0.021 | 0.265 | 3.69 | Y | 70^3 | 14.4 | 10.08 | 0.54 | 4.4 | 0.7 |
| Run 10 | 246.4 | 151.2 | 0.02 | 0.021 | 0.265 | 4.11 | N | 100^3 | 14.4 | 0 | 0.54 | 0 | 0 |

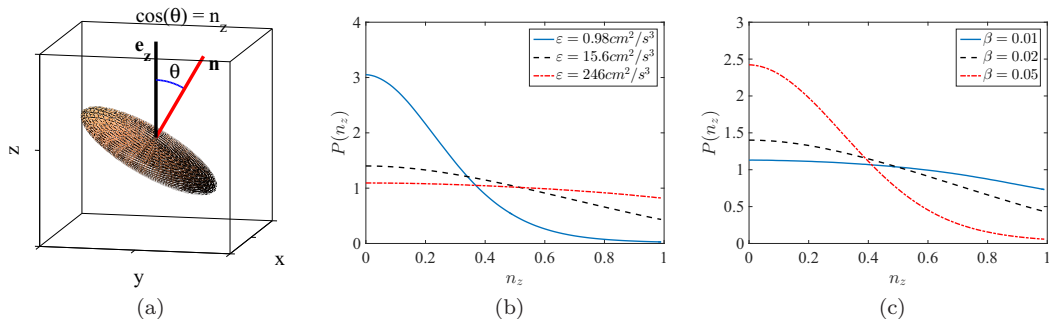


FIG. 1. (a) Illustration of the definition of the vector \mathbf{n} parallel to the small axis of the ellipsoid. The angle θ is the angle between \mathbf{n} and the direction of gravity, \mathbf{g} . With our definition, $\cos(\theta) = n_z$. We restrict ourselves to $0 \leq n_z \leq 1$. (b) Distribution of n_z for ellipsoids with aspect ratio $\beta = 0.02$ in the presence of gravity in a turbulent flow at $\varepsilon \approx 1 \text{ cm}^2/\text{s}^3$ (full line), $\varepsilon \approx 16 \text{ cm}^2/\text{s}^3$ (dashed line), and $\varepsilon \approx 256 \text{ cm}^2/\text{s}^3$ (dashed-dotted line). (c) Distribution of n_z in the presence of gravity, at $\text{Re}_\lambda = 95$, for ellipsoids of aspect ratio $\beta = 0.01$ (full line), $\beta = 0.02$ (dashed line), and $\beta = 0.05$ (dashed-dotted line).

spherical particles, inertial effects become important for $\text{St} \approx 0.4$, i.e., in the range covered by the present study [20,34]. This aspect will be further discussed in Sec. IV D.

The values of $S_{v,s}$ shown in Table II are all larger than 1, which suggests that gravitational settling plays a dominant role in all our simulations. Comparing the settling velocity with the rms of the turbulent velocity fluctuations suggests, however, that the role of turbulence becomes more prevalent at $\varepsilon \approx 16 \text{ cm}^2/\text{s}^3$ and $\beta = 0.01$, or at $\varepsilon \approx 256 \text{ cm}^2/\text{s}^3$ and $\beta = 0.02$ ($S_{v,L} < 1$). These issues will be further discussed in Sec. III, in particular Sec. III C.

As already stressed, the equations of motion for the crystals have been derived by neglecting the fluid inertia, i.e., by assuming a very small Reynolds number of the particles. Actually, by judging from the quantities listed in Table II, the Reynolds number based on the settling velocities is here close to unity. The corrections due to a nonzero Reynolds number of the particle have been the subject of several investigations [35,36]. Taking into account finite Reynolds number effects may be particularly important, in particular for the description of the rotational degrees of freedom [11,37,38]. We note that the torque acting on oblate ellipsoids, and due to finite Reynolds number effects (deviation from the Stokes regime), tends to stabilize the configuration where the ellipsoid settles with its basis horizontal [1,35,39]. How the effects of inertia would affect the equation of motion for the angular degrees of freedom is unknown. Having completely neglected these effects is certainly a limitation of the present approach.

III. ORIENTATION AND SETTLING STATISTICS OF ELLIPSOIDS IN TURBULENT FLOWS

From a geometric point of view, the oblate ellipsoids considered in this study can be characterized by the angle between the gravity, \mathbf{g} , and the short eigendirection of the ellipsoid, \mathbf{n} . We define the unit vector \mathbf{e}_z of the (fixed) frame of reference as $\mathbf{e}_z = -\mathbf{g}/|\mathbf{g}|$. As represented in Fig. 1(a), the cosine between \mathbf{n} and \mathbf{g} , or equivalently, \mathbf{e}_z , therefore reduces to n_z , up to an immaterial sign. We chose the sign of n_z , by convention, to be positive throughout.

A. Orientation statistics

In this subsection, we focus on the distribution of the orientation of the ellipsoid with respect to \mathbf{g} , which is relevant not only to the study of collisions, but also to understand the reflection properties of light by clouds loaded with ice crystals [40,41].

The results presented in this subsection are generally in agreement with those of Ref. [10] and can be understood theoretically with the help of the formalism developed in Ref. [42]. This theoretical

approach leads to a quantitative description of the probability distribution functions (PDF) [12]. In the following, we briefly discuss the distribution of n_z for ellipsoids with an aspect ratio $\beta = 0.02$, at the three values of ε simulated, and as a function of β , at $\varepsilon \approx 16 \text{ cm}^2/\text{s}^3$.

Figure 1(b) shows the distribution of n_z for ellipsoids of aspect ratio $\beta = 0.02$, at the three Reynolds numbers considered here, in the presence of gravity. In contrast, the distribution of n_z is uniformly distributed in the absence of gravity. At low Reynolds number, the probability distribution is strongly biased towards small values of n_z , corresponding to ellipsoids settling edge first, which in effect minimizes the drag in the vertical direction. The effect strongly diminishes when the Reynolds number increases, as demonstrated in Fig. 1(b): at the highest Reynolds number simulated in this work, $\text{Re}_\lambda = 151$, the angles n_z are almost uniformly distributed; the corresponding curve differs from 1 by no more than 10%. The observed tendency to relax towards a uniform distribution of n_z when the intensity of turbulence, i.e., the energy dissipated in the fluid ε increases, can be qualitatively understood from the increase of the torque exerted by the turbulent flow on the particles; see Eq. (5).

Figure 1(c) shows the distribution of orientation of the ellipsoids settling in a turbulent flow at intermediate Reynolds number ($\varepsilon \approx 16 \text{ cm}^2/\text{s}^3$, $\text{Re}_\lambda = 95$). The main observation is that the ellipsoids with the highest values of β are those whose distribution of n_z is most biased towards small values; see the dashed-dotted line in Fig. 1(c). In contrast, for ellipsoids with the smallest value of β , the distribution of n_z is almost uniform; see the full line in Fig. 1(c). The trend shown in Fig. 1(c) can be qualitatively understood by noticing that the mass and the inertia of the ellipsoids increase with β . Therefore, at a given turbulence intensity, the randomizing effect of the flow is felt more strongly when β becomes smaller. In this sense, the trends observed in Figs. 1(b) and 1(c) both illustrate that turbulence tends to randomize the direction of the ellipsoids, the more so as the Reynolds number of the turbulent flow increases, and as the inertia of the ellipsoids decreases.

The simplified model used here, which completely neglects corrections due to fluid inertia (finite Reynolds numbers effects), predicts that particles may settle with *any* orientation in a fluid at rest. In this sense, our numerical results show that this degeneracy is lifted by turbulence, at least over an intermediate range of values. This effect can be explained quantitatively [12]. Taking into account the corrections due to fluid inertia, in a systematic expansion in the Reynolds number of the particle, leads to corrections that would favor settling of the ellipsoids with $n_z \approx 1$ [1,39]. This may be a limitation of the present work. However, the lack of a set of equations taking systematically into account the corrections due to inertia, even at the lowest Reynolds number, makes it difficult to analyze the problem completely. Similar difficulties occur when studying the settling of elongated (prolate) ellipsoids in a flow; see, e.g., Ref. [11].

We conclude this subsection by pointing out that our study leaves aside interesting properties concerning the correlation between the orientation of the ellipsoids, \mathbf{n} , and the velocity gradient tensor or the tumbling rate ($\langle \dot{\mathbf{n}}^2 \rangle$). These have been recently studied in various cases, mostly when the angular dynamics is overdamped and in the absence of gravity [9,43–47].

B. Orientation dynamics

To obtain information on the dynamics of the vector \mathbf{n} , we determined the correlation function, $\mathcal{C}(t; \tau) \equiv \langle \mathbf{n}(t)\mathbf{n}(t + \tau) \rangle$, where the average in the definition of \mathcal{C} is taken over an ensemble of ellipsoids. As the dynamics of the ellipsoids in the flow is statistically stationary, the correlation function depends only on the time separation between the two instants, τ : $\mathcal{C}(t; \tau) = \mathcal{C}(\tau) = \langle \mathbf{n}(0)\mathbf{n}(\tau) \rangle$.

Figure 2 shows the correlation functions plotted as a function of τ/τ_K , for ellipsoids with $\beta = 0.02$, both in the presence (top panel) and in the absence (lower panel) of gravitational settling. In all cases considered, the correlation function does not reveal any sign of a secondary maximum (a peak) for $\tau > 0$. The crystals therefore do not show any sign of oscillations. This is consistent with the representation of the motion in Ref. [15]; see in particular their Fig. 4(a). This property may change when taking into account the effect of fluid inertia [39].

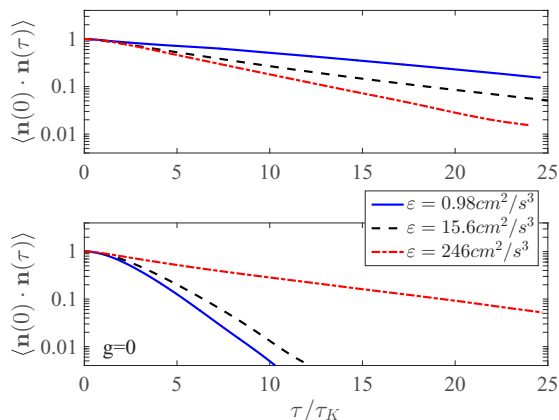


FIG. 2. Correlation function of the vector \mathbf{n} in the flow in the presence (upper panel) and in the absence (lower panel) of gravitational settling for ellipsoids with an aspect ratio $\beta = 0.02$. The correlation function $\langle \mathbf{n}(0)\mathbf{n}(\tau) \rangle$ is plotted as a function of τ/τ_K .

In all cases shown in Fig. 2, the correlation function decays to a value of order $1/e$ over a time of decorrelation, $\tau_{C,n}$ which is in the range $6.2 \lesssim \tau_{C,n}/\tau_K \lesssim 14.3$ with, and $3.1 \lesssim \tau_{C,n}/\tau_K \lesssim 7.8$ without, gravitational settling. In all cases considered here, the orientation of the ellipsoids varies over a characteristic time of a few τ_K . The correlation function strongly depends on ε and on the presence or absence of gravitational settling. Whereas at small turbulence intensity ($\varepsilon \approx 1 \text{ cm}^2/\text{s}^3$) \mathbf{n} decorrelates much faster in the absence than in the presence of settling, the trend is completely opposite at much higher ε . As a general trend, the correlation function, once expressed in units of τ/τ_K , decays faster (slower) when ε increases in the presence (absence) of gravity.

C. Settling velocity

In a still flow, the settling velocity depends on the value of n_z . The dependence of the settling velocity of the ellipsoids (absolute value of $\langle v_z \rangle$) as a function of n_z is shown in Fig. 3(a), as a curve with cross symbols, when $\beta = 0.02$. The qualitative feature of Fig. 3(a) can be understood by looking for steady solutions of Eq. (6) assuming $\mathbf{u} = 0$ and a fixed orientation of the ellipsoids. The settling velocity becomes smaller when the value of n_z increases, which is a consequence of the increased resistance of the fluid as the largest sides of the ellipsoids become closer to horizontal.

It has already been documented that turbulence may change the settling velocity of droplets in a turbulent flow; see, e.g., Ref. [48]. Figure 3(a) shows the dependence of the settling velocity, $U_{\text{sett}} = -\langle v_z \rangle$, conditioned on the angle n_z , for the three Reynolds numbers studied here. As the turbulence intensity ε increases, the dependence of the averaged settling velocity conditioned on the ellipsoid orientation n_z shows a clear variation. Specifically, the settling velocity of the ellipsoids, at small values of n_z , significantly increases with ε . On the other hand, the slowest settling velocities, when $n_z \approx 1$, decrease when ε increases. Averaged over all possible directions, the settling velocity U_{sett} shows a weak variation as a function of the turbulence intensity: it is $\approx 9.6 \text{ cm/s}$ for $\varepsilon \approx 1 \text{ cm}^2/\text{s}^3$, $\approx 9.8 \text{ cm/s}$ for $\varepsilon \approx 16 \text{ cm}^2/\text{s}^3$, and $\approx 10.1 \text{ cm/s}$ for $\varepsilon \approx 256 \text{ cm}^2/\text{s}^3$. Overall, these slight variations of U_{sett} are consistent with those reported in Ref. [10]. Figure 3(a) implies that two particles very close to each other may have a very significant velocity difference, provided the two ellipsoids have a different orientation. This effect becomes slightly stronger when ε increases. In a suspension of identical particles, in the absence of gravity, the velocity differences between particles close to each other is much smaller. This difference is at the origin of the very different collision rates obtained in the presence and in the absence of gravity, reported in the following section.

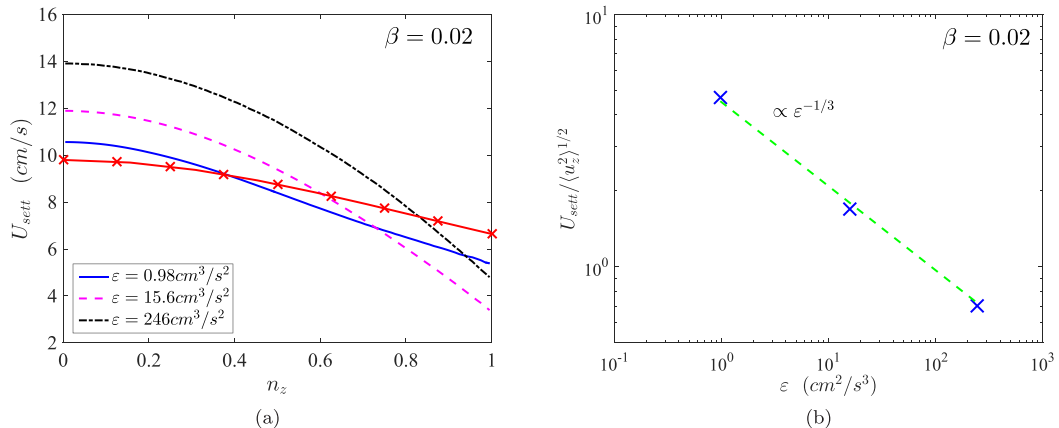


FIG. 3. Averaged settling velocity of ellipsoids in turbulent flows: (a) settling velocity as a function of n_z for ellipsoids with an aspect ratio $\beta = 0.02$, at several values of ε , as indicated in the legend (for comparison, the settling velocity in still air is shown by the curve with crosses); (b) ratio between the settling velocity and the rms of the fluctuations. This ratio, which is very close to the gravity parameter $S_{v,L}$, defined by Eq. (10), is shown for $\beta = 0.02$, as a function of ε . The dashed line indicates the $\varepsilon^{-1/3}$ dependence, which captures qualitatively the dependence obtained numerically.

In the range of values of β considered here, $0.01 \leq \beta \leq 0.05$, at a fixed value of the energy dissipation rate in the flow, $\varepsilon \approx 16 \text{ cm}^2/\text{s}^3$, the settling velocity is found to increase linearly with β . This can be readily understood by noticing that the ellipsoids considered here have a fixed value of a , so their volumes, hence their masses, are proportional to β . In the limit of very thin ellipsoids, relevant to our study, the resistance tensor $\hat{\mathbf{K}}$ defined by Eq. (4) is independent of β . The settling velocity is therefore proportional to the mass, hence to β , consistent with the results shown in Table II.

The theoretical work of Ref. [12] suggests that the proper gravity parameter to parametrize the bias is rather $S_{v,L}$, defined by Eq. (10). On general grounds, the variance of the velocity fluctuations of the flow, $\langle u_z^2 \rangle$ is related to the dissipation, ε , and the integral length scale of the flow, L , as

$$\langle \mathbf{u}^2 \rangle \propto (\varepsilon L)^{2/3}. \quad (11)$$

This relation implies that the ratio between the settling velocity, which does not vary much with the Reynolds number, and the rms of the velocity fluctuations should roughly go as $\propto \varepsilon^{-1/3}$ (note that in the case of spherical particles at Stokes numbers comparable to those considered here, the variance of the velocity of the fluid and of the particles are very close to each other [49]). This expectation is consistent with our own numerical findings; see Fig. 3(b) (the size of the integral length scale of the velocity here is ≈ 5 cm). The range of values of ε considered here covers cases where the settling velocity is larger than the rms of the turbulent velocity fluctuations ($\varepsilon \approx 1 \text{ cm}^2/\text{s}^3$), where the two velocities are comparable ($\varepsilon \approx 16 \text{ cm}^2/\text{s}^3$), and where the turbulent fluctuations dominate ($\varepsilon \approx 256 \text{ cm}^2/\text{s}^3$). When $\varepsilon \approx 16 \text{ cm}^2/\text{s}^3$, we find that the settling velocity is larger (smaller) than the rms of the turbulent velocity fluctuations when $\beta = 0.05$ ($\beta = 0.01$).

Further insight into the fluctuations of the settling velocity and its dependence on the orientation, n_z , is provided by Fig. 4. The figure shows the joint PDF of v_z (the vertical velocity) and n_z for ellipsoids of aspect ratio $\beta = 0.02$ at the three turbulence intensities considered. The conditional value of v_z on n_z , $\langle v_z | n_z \rangle$ is shown as a full line. The vertical extent of the region with a large probability is, up to a numerical prefactor, the rms of the velocity fluctuations. At the smallest turbulence intensity, $\varepsilon \approx 1 \text{ cm}^2/\text{s}^3$ (see the left panel of Fig. 4), the fluctuations in the vertical velocities are small compared to $\langle v_z | n_z \rangle$. In particular, the vertical velocity is almost always negative, implying that almost all particles move downward, in the direction imposed by gravity. In contrast, at much larger turbulence intensity (see the right panel of Fig. 4), the velocity fluctuations are large

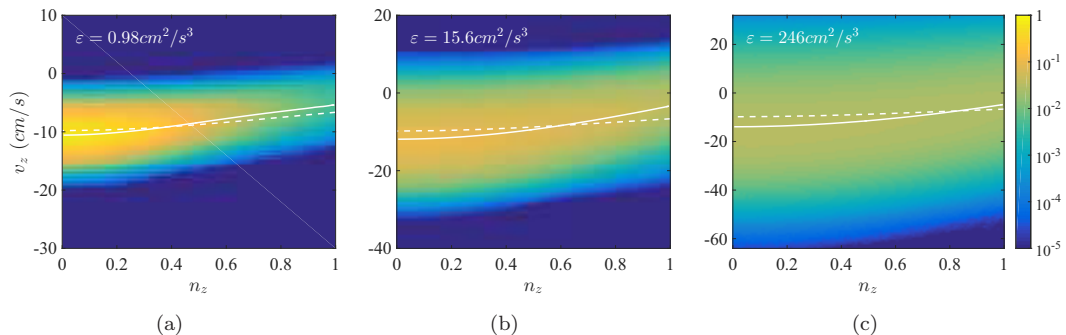


FIG. 4. Comparison between velocity fluctuations and settling velocity at different turbulence intensity. The figure shows the joint PDFs of the orientation, n_z (horizontal) and of the vertical velocity, v_z (vertical) for ellipsoids at $\beta = 0.02$, at the three values of ε , as indicated. The probability is color coded, as indicated on the color bar. The conditional average $\langle v_z | n_z \rangle$ is indicated by the full line in the figure (the dashed line shows the settling velocity in still fluid).

compared to $\langle v_z | n_z \rangle$, which implies that while ellipsoids move downward, on the mean, they have also large probabilities of moving up. The intermediate case, $\text{Re}_\lambda = 95$, shown in the middle panel of Fig. 4, corresponds to a case where ellipsoids can, with a relatively small probability, move up in the gravity field.

Figure 4 clearly shows that, as expected, the importance of the bias due to settling diminishes when the turbulence intensity, ε , increases. Although the gravity parameter corresponding to ellipsoids of aspect ratios $\beta = 0.02$ at the highest turbulence intensity considered ($\varepsilon \approx 256 \text{ cm}^2/\text{s}^3$), is as high as $S_{v,s} \approx 4.4$, the bias induced by settling is actually relatively small. Consistent with this observation, the results presented in Sec. IV show that the collision rates at $\varepsilon \approx 256 \text{ cm}^2/\text{s}^3$ with and without gravitational settling do not differ very much. This provides additional reason to measure the influence of gravity using $S_{v,L}$, which is smaller than 1 for $\varepsilon \approx 256 \text{ cm}^2/\text{s}^3$, rather than $S_{v,s}$.

IV. COLLISIONS

A. Definition of the collision rates

The probability of collisions between identical particles can be conveniently expressed in terms of the collision kernel, K , defined by expressing the number of collisions N_c over a time T , in a volume V containing N particles ($N \gg 1$) as

$$N_c = \frac{1}{2} K \times \frac{N^2}{V} \times T. \quad (12)$$

The collision kernel has therefore the dimension of the cube of a length (a volume) divided by a time. It depends on the Reynolds number, the shape of the particles, and the gravity acceleration.

Over the years, a good understanding of the collision rate in a turbulent, monodisperse suspension of spherical particles has been obtained. The pioneering work of Saffman and Turner [50] provides an explicit expression for the collision rate in the case of spherical droplets which exactly follow the flow. In the case of inertial particles, the collision rate is enhanced due to, on the one hand, an enhanced concentration of particles around existing particles in the suspension [16], and, on the other hand, a much increased relative velocity of the particles when they collide [18,19]. Numerical studies indicate that the latter effect prevails in determining the collision rate in a turbulent suspension as soon as the inertia of the particles is significant [20,34].

Interestingly, several simulations have pointed that at a fixed turbulence rate, the effect of gravitational settling is to *reduce* the collision rate of spherical particles [26,51–53].

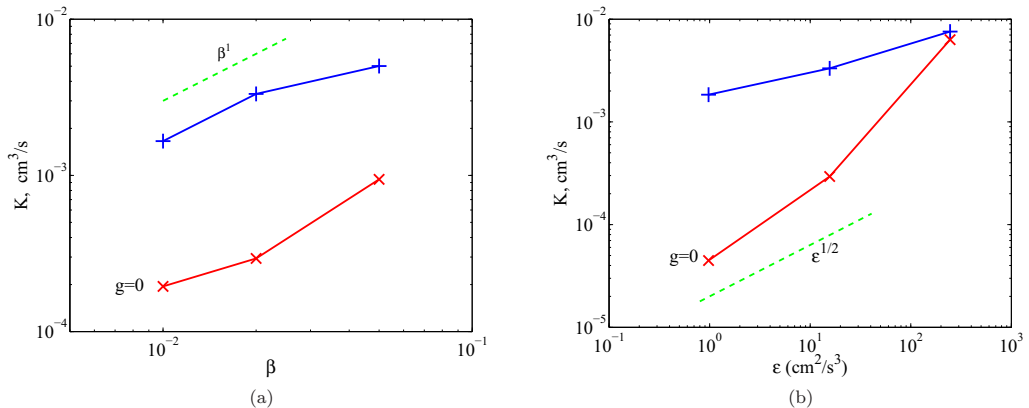


FIG. 5. Collision rate of a suspension of ellipsoids. The collision rates in the presence (“+” symbols) and in the absence (“x” symbols) of gravitational settling are compared. (a) Collision rate as a function of β , at a fixed Reynolds number, $\text{Re}_\lambda = 95$ ($\epsilon \approx 16 \text{ cm}^2/\text{s}^3$). The collision rate increases slightly with β in both cases and is much larger in the presence of gravity. (b) Collision rate as a function of ϵ , at a fixed value of $\beta = 0.02$. Generally the collision rates in the absence of gravity (shown with a “x” symbol) are much smaller than in the presence of gravity (shown with a “+” symbol). The difference however, diminishes when ϵ increases.

B. Collision rate statistics

The collision kernel, K , expressed in cm^3/s and measured from our own DNS, is shown in Fig. 5 as a function of the dissipation rate ϵ in the fluid, both in the presence and in the absence of gravitational settling.

The collision rate is first shown as a function of β , at the intermediate value of $\epsilon \approx 16 \text{ cm}^2/\text{s}^3$; see Fig. 5(a). The collision rate is much smaller in the absence than in the presence of gravity. The increase of the collision kernel by a factor $\gtrsim 10$ due to gravity sharply contrasts with the *decrease* of the collision kernel observed at comparable Reynolds numbers in the case of spherical particles [52,53]. Figure 5(a) indicates an increase, essentially linear, of the collision rate as a function of β .

Figure 5(b) shows the collision rate as a function of the energy dissipation, ϵ , and demonstrates once again that at small Reynolds numbers, the collision kernel is vastly enhanced by the presence of gravity. It is, at the smallest value of ϵ considered here ($\epsilon \approx 1 \text{ cm}^2/\text{s}^3$), ~ 40 times larger in the presence of gravity, than without it. The ratio, however, significantly drops when increasing the Reynolds number, and at the highest Reynolds number here ($\epsilon \approx 256 \text{ cm}^2/\text{s}^3$), the ratio is only slightly larger than 1.

In Sec. IV D we will discuss the physical mechanisms possibly responsible for the behavior shown in Fig. 5.

C. Orientation of colliding ellipsoids in the presence of gravity

As already explained (see Sec. III C), the dependence of the settling velocity on the angle between the ellipsoid and the direction of gravity naturally provides a dispersion of the relative velocity of the particles close to each other, thus potentially enhancing the collision rate.

To explore further these issues, Figs. 6(a)–6(c) show the orientation of two colliding ellipsoids, at the three Reynolds numbers considered. The continuous line shows the PDF of the orientations of all the ellipsoids. We distinguish the two colliding ellipsoids by identifying the one which has, at the time of the collision, the highest position of its center of mass. The distribution of the angles n_z for the upper ellipsoid is shown as a dashed line, whereas the distribution for the lower ellipsoid is shown as a dashed-dotted line. Overall, Fig. 6 shows that the higher ellipsoid tends to have predominantly a smaller value of n_z than the lower ellipsoid, whose probability of orientation has more weight at

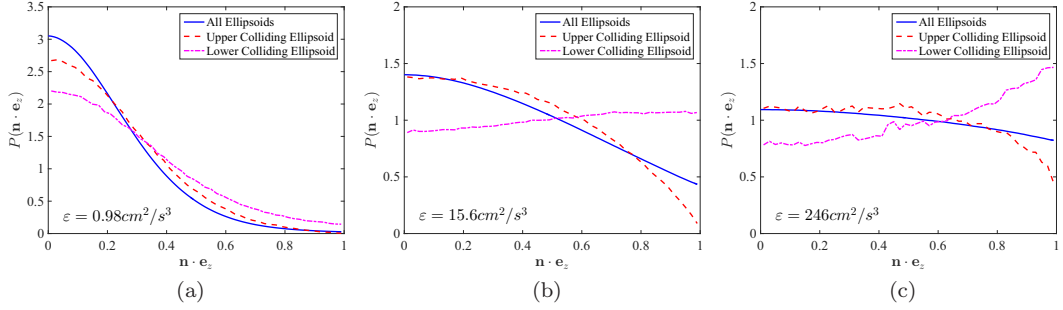


FIG. 6. Distribution of n_z for the colliding ellipsoids during their collision: upper ellipsoid (dashed red line) and lower ellipsoid (dashed-dotted magenta line). As a comparison, the distribution of the angles for all ellipsoids is shown with a full line. The Reynolds number increases from $\text{Re}_\lambda = 56$ (left), $\text{Re}_\lambda = 95$ (center), and $\text{Re}_\lambda = 151$ (right). The results are shown for ellipsoids with $\beta = 0.02$. The upper (lower) ellipsoids have a larger probability of having a small (large) value of n_z , which implies that the upper ellipsoids settle faster than the lower ones.

larger values of n_z . This tendency persists for all the values of ε considered in this study. For the two largest values of Re_λ considered, the probability of orientation of the lower ellipsoids has even more weight at larger values of n_z than at smaller ones.

In comparison, Fig. 7 shows the distribution of the relative angle between the two colliding ellipsoids, both in the presence and in the absence of gravitational settling. Specifically, Fig. 7 shows the cumulative PDF, defined as

$$\Pi(\xi) = \int_0^\xi P(\xi') d\xi', \quad (13)$$

where $P(\xi)$ is the PDF of the cosine of the angle $(\mathbf{n}_1 \cdot \mathbf{n}_2)$ between the vectors $\mathbf{n}_{1,2}$ characterizing the orientations of the two ellipsoids. In all cases, Fig. 7 shows a sharp increase of Π close to $\mathbf{n}_1 \cdot \mathbf{n}_2 = 1$, that is, for perfectly aligned ellipsoids [the PDF $P(\xi)$ shows a very narrow peak near $\xi = 1$]. This corresponds to a very high probability of the two ellipsoids colliding while perfectly aligned with

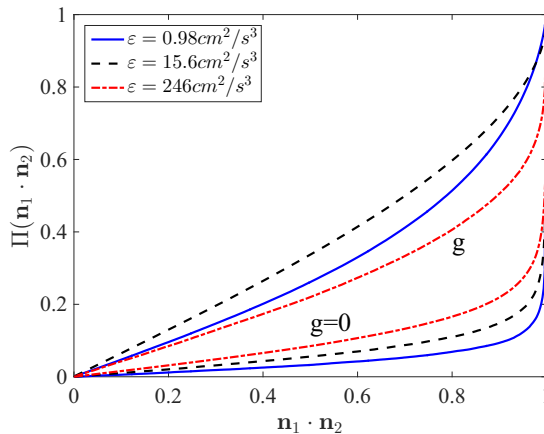


FIG. 7. Cumulative probability distribution function of the cosine of the relative angle between two colliding ellipsoids, $\mathbf{n}_1 \cdot \mathbf{n}_2$. The full, dashed, and dashed-dotted lines correspond to $\text{Re}_\lambda = 56$, $\text{Re}_\lambda = 95$, and $\text{Re}_\lambda = 151$, respectively. The three lowest (respectively highest) curves correspond to a case without (respectively with) gravitational settling. The cumulative probability distribution function is defined by Eq. (13).

each other. The probability of the two ellipsoids colliding at a finite angle is clearly larger in the case with gravity than in the case without gravity. This is consistent with the fact that in the presence of gravity, many collisions occur due to a differential gravitational settling. While this difference is visible at each of the three Reynolds numbers investigated, Fig. 7 shows that the difference becomes weaker at the highest Reynolds number studied. This is consistent with the fact that, as the effect of turbulence becomes stronger compared to that of gravitational settling, the difference in the nature of the collisions between the two cases diminishes.

D. Discussion

To provide an explanation of the dependence of the collision rate K on ε and β shown in Fig. 5, we begin by recalling that the collision kernel can be interpreted as a flux of particles incoming into one of them. While this flux can be explicitly computed in the case of colliding spheres, an exact determination of the collision rate is much more difficult in the problem of colliding ellipsoids considered here. Still, as we show in this subsection, the interpretation in terms of a flux allows us to provide qualitative estimates, as well as a qualitative explanation of the trends observed in Secs. IV B and IV C.

1. Influence of gravitational settling

Consider first the case of ellipsoids in the presence of gravitational settling. As stressed in Sec. III C, gravitational settling induces a strong relative velocity difference between ellipsoids with a different orientation; see Fig. 3. Based on Eq. (6), the velocity difference is expected to be proportional to $2\beta g\tau_{sp}$. The values shown in Fig. 3 suggest a value of the velocity differences $\Delta u_s \approx \beta g\tau_{sp}/5$, which leads to $\Delta u_s \approx 1.1$ cm/s. The flux of particles incoming into an oblate ellipsoid can be estimated as the product of the area of its largest side, $\sim\pi a^2$, and of the relative velocity between two objects. This provides, as an estimate of the collision rate of the particles, $K \approx \frac{\pi}{5}a^2\beta g\tau_{sp}$. In the case of ellipsoids with $\beta = 0.02$ and $\varepsilon \approx 16$ cm²/s³, this leads to $K \approx 8 \times 10^{-4}$ cm³/s, which provides the right order of magnitude for the value of K determined numerically, $K \approx 3.3 \times 10^{-4}$ cm³/s [see Fig. 5(b)]. The estimate above for the collision rate also predicts a growth of $K \propto \beta$. This is certainly consistent with the trend observed at $\varepsilon \approx 16$ cm²/s³, between $\beta = 0.01$ and $\beta = 0.02$. The growth of K is slower between $\beta = 0.02$ and $\beta = 0.05$, which can be understood as a consequence of the increased importance of inertia, as explained below. Last, the estimate above does not involve the intensity of turbulence, ε . This is qualitatively consistent with the relatively weak increase of K , when $\beta = 0.02$, as ε increases from 1 cm²/s³ to 256 cm²/s³.

2. Influence of turbulence in the absence of gravitational settling

We now turn to estimating the collision rate in the absence of gravitational settling, and begin with the case where the motion of the ellipsoids can be thought of as a simple advection by the flow. This picture is expected to be correct when the relaxation time of the particles is very short compared to the time of the turbulent eddies, i.e., when the Stokes number St is very small. In this case, the collision between particles is due to the relative motion between two ellipsoids, which in turn results from the velocity gradients. Specifically, two objects separated by a distance a , small compared to the Kolmogorov length, have a relative velocity $\propto a/\tau_K$ [20,50], where $\tau_K = (v/\varepsilon)^{1/2}$ is the Kolmogorov time. This leads to an estimate of $K \approx \pi a^3(\varepsilon/v)^{1/2}$. The corresponding numerical values are $K \approx 3 \times 10^{-5}$ cm³/s when $\varepsilon \approx 1$ cm²/s³ and $K \approx 1.2 \times 10^{-4}$ cm³/s when $\varepsilon \approx 16$ cm²/s³. These values only slightly underestimate the collision rate determined numerically in the absence of gravity; see the lower curve of Fig. 5(b). Our estimate also predicts a dependence of $K \propto \varepsilon^{1/2}$ (all other parameters being fixed). This is close to the dependence observed in the range 1 cm²/s³ $\leq \varepsilon \leq 16$ cm²/s³. In sharp contrast, this estimate is inappropriate to explain the collision rate at $\varepsilon \approx 256$ cm²/s³ and the fact that, in the absence of gravitational settling, the collision kernel K grows much faster than $K \propto \varepsilon^{1/2}$ in the range 16 cm²/s³ $\lesssim \varepsilon \lesssim 256$ cm²/s³; see Fig. 5(b).

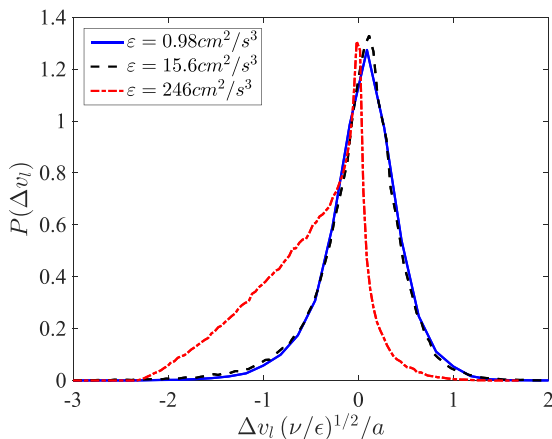


FIG. 8. Probability distribution function of the relative velocity between the center of mass of two colliding ellipsoids in the absence of gravity. The full, dashed, and dashed-dotted lines correspond to $\varepsilon \approx 1 \text{ cm}^2/\text{s}^3$, $\varepsilon \approx 16 \text{ cm}^2/\text{s}^3$, and $\varepsilon \approx 256 \text{ cm}^2/\text{s}^3$, respectively. Although the distributions for $\varepsilon \approx 1 \text{ cm}^2/\text{s}^3$ and $\varepsilon \approx 16 \text{ cm}^2/\text{s}^3$ are symmetric and do not extend much beyond $\Delta v_l/[a(\varepsilon/\nu)^{1/2}]$, the one obtained for $\varepsilon \approx 256 \text{ cm}^2/\text{s}^3$ displays a broad tail for negative values of the relative velocity, thereby revealing the presence of large inertial effects.

We note that the estimates for K , with and without gravitational settling, obtained by neglecting the particles inertia make possible a direct comparison between the effects of differential settling and the effect of turbulence. Determining when $K \approx \frac{\pi}{5} a^2 \beta g \tau_{sp}$ and $K \approx a^3/\tau_K$ become comparable leads to the conclusion that the effect of gravitational settling should become negligible compared to that of turbulence when $a/\tau_K \gtrsim \beta g \tau_{sp}$, or equivalently, $\varepsilon \gtrsim \nu(\beta g \tau_{sp}/a)^2$. With the parameter value $\beta = 0.02$, this points to a value of $\varepsilon \approx 500 \text{ cm}^2/\text{s}^3$. As we now argue, this argument overestimates the value of ε at which turbulence becomes dominant, as inertial effects have been so far completely ignored.

3. Inertial effects

The strong deviation from the qualitative prediction that $K \approx a^3/\tau_K$ actually points to the importance of inertial effects. In turbulent suspensions of spherical droplets, similar deviations are known to occur when the inertia of the particles, measured by the Stokes number [Eq. (8)] increases [16,18–20]. The very substantial increase of the collision rate can be attributed either to the effect of the preferential concentration of droplets in certain regions of the flow or to the increased relative velocity between close particles (the “sling effect” [18,51]). Careful numerical results establish that the latter effect plays the dominant role in the increase of the collision rate [34], as soon as the Stokes number of the particles $St = \tau_{sp}/\tau_K \gtrsim 0.5$, where $\tau_{sp} = 2/9(r^2/\nu)(\rho_p/\rho_f)$, where a is the radius of the spheres. As indicated in Table II, the Stokes number of the particles considered in the present study is of order 0.5 at the highest value of ε simulated here.

To demonstrate the role of the sling effect in the observed growth of the collision rate when the kinetic energy injection increases from $\varepsilon \approx 16 \text{ cm}^2/\text{s}^3$ to $\varepsilon \approx 256 \text{ cm}^2/\text{s}^3$, Fig. 8 shows the PDF of the relative velocity between the centers of mass of two colliding ellipsoids, in the absence of gravity. Specifically, when two ellipsoids with centers of mass \mathbf{x}_1 and \mathbf{x}_2 , and velocities \mathbf{v}_1 and \mathbf{v}_2 ($\mathbf{v}_i = d\mathbf{x}_i/dt$) collide, we define Δv_l as $\Delta v_l \equiv (\mathbf{v}_2 - \mathbf{v}_1) \cdot (\mathbf{x}_2 - \mathbf{x}_1)/\|\mathbf{x}_2 - \mathbf{x}_1\|$. In the absence of any inertial effect, the fluctuations of Δv_l scale as $\langle (\Delta v_l)^2 \rangle \approx a^2(\varepsilon/\nu)$. For this reason, Fig. 8 shows the PDF of $\Delta v_l/[a(\varepsilon/\nu)^{1/2}]$. With this scaling, the PDF of Δv_l superpose very well when $\varepsilon \approx 1 \text{ cm}^2/\text{s}^3$ and $\varepsilon \approx 16 \text{ cm}^2/\text{s}^3$. The corresponding distributions are peaked around ≈ 0 and do not extend much beyond $\Delta v_l/[a(\varepsilon/\nu)^{1/2}]$, thus demonstrating that ellipsoids collide with a velocity difference of order $a(\varepsilon/\nu)^{1/2}$, which is consistent with the absence of significant inertial effect. Note

that, contrary to the case of colliding spheres, the relative velocity between the centers of mass, Δv_l , can be *positive* when the ellipsoids collide: Even when their centers of mass move away from each other ($\Delta v_l > 0$), the ellipsoids may come into contact as a consequence of the angular motion. The distribution of Δv_l when $\varepsilon \approx 256 \text{ cm}^2/\text{s}^3$, however, strongly differs from the distributions at lower values of ε . The main peak around $\Delta v_l = 0$ is narrower, and very strikingly, the PDF acquires a broad tail towards $\Delta v_l < 0$. This shows that when $\varepsilon \approx 256 \text{ cm}^2/\text{s}^3$, colliding ellipsoids move, with a significant probability, with a relative velocity much larger than the fluid one. This is a clear signature of large inertial effects, consistent with the well-documented sling effect [34].

The results concerning collisions in droplet suspensions then provide an explanation for the very sharp increase of K for particles with $\beta = 0.02$, between $\varepsilon \approx 16 \text{ cm}^2/\text{s}^3$ ($\text{St} \approx 0.135$) and $\varepsilon \approx 256 \text{ cm}^2/\text{s}^3$ ($\text{St} = 0.54$). We also note that the Stokes number for particles with $\beta = 0.05$ and $\varepsilon \approx 16 \text{ cm}^2/\text{s}^3$ is $\text{St} \approx 0.34$, which points to significant effects of particle inertia, and could explain the significant difference between the collision rates K between $\beta = 0.02$ and $\beta = 0.05$, in the absence of gravity. It may also explain the departure from the linear dependence on β , in the presence of gravity, when β increases to 0.5, as the effects of turbulence become important. Distinguishing quantitatively the effect of differential settling from that of inertia in this case, however, is likely to be a challenging task.

V. CONCLUSIONS

In this work, we have considered the collision of oblate ellipsoids, of properties close to those of ice crystals, in a turbulent flow whose intensity ranges from $\approx 1 \text{ cm}^2/\text{s}^3$ to $\approx 256 \text{ cm}^2/\text{s}^3$. The parameters chosen here are close to those observed in moderately turbulent clouds. The motion of the ellipsoids is determined numerically by solving the equations determining their translation and rotation. These equations use the expressions of the force and torque derived in the limit where the Reynolds number of the flow around the object is very small. The collision rate has been determined using the ghost-particle approximation, i.e., by following independent trajectories of ellipsoids, and determining when they collide in the flow.

In the presence of gravity, our results show that crystals tend to settle edge first. We also observed a strong variation of the settling velocity with the orientation, qualitatively consistent with the observed gravitational settling in still air. Over the range of studied turbulence intensity, this effect tends to increase with ε . On the other hand, the alignment effect of the ellipsoid with gravity, \mathbf{g} , tends to diminish when the intensity of turbulence increases. This can be attributed to an associated increase in the velocity gradients in the flow, which in turn leads to an enhanced torque acting on the ellipsoid.

Our study points to the competition between several physical effects which strongly influence the collision rate. As pointed out already [15], differential gravitational settling plays a very important role, in particular at very small Reynolds numbers ($\varepsilon \approx 1 \text{ cm}^2/\text{s}^3$). In this regime, a direct comparison between collision rate with and without gravitational settling reveals that the collision rate is reduced by almost two orders of magnitude in the absence of \mathbf{g} . As ε increases, however, the collision rate induced in the turbulent flow without gravitational settling increases very rapidly, so the relative influence of \mathbf{g} rapidly decreases: at $\varepsilon \approx 256 \text{ cm}^2/\text{s}^3$, the collision rates with and without \mathbf{g} are very close. Thus, the very strong effect of gravitational settling seems to be limited to small Reynolds numbers. Although the role of gravitational settling becomes weaker when the turbulence intensity increases, the analysis of the relative orientation between two colliding ellipsoids reveals that the influence of gravity remains significant, even at the highest value of ε considered here.

It is not completely clear whether at still higher values of the turbulence intensity, gravitational settling will still increase the collision kernel, as is the case over the range of values of ε considered here, or whether it will in fact *lower* the collision rate, as happens for droplets [52,53].

The model used here, based on a set of equations which do not take into account any inertia correction, predicts in agreement with previous work [10,12] a tendency of the ellipsoids to settle with their edges first. This clearly differs from the expectation based on the torque due to the corrections induced by the fluid inertia [35,39]. Given that the values of the Reynolds number based on the settling

velocity are not very small, it would be important to understand in detail the role of fluid inertia on the effects discussed in this work. Qualitatively, the conclusion reached in this work, namely, that the collision rate between crystals is due to differential settling at small Reynolds number, and to turbulence at higher Reynolds number, is very unlikely to depend very sensitively on the precise nature of the distribution of orientation of the ellipsoids.

Although we have chosen realistic values of the characteristic small time and length scales of the turbulent flow in the present calculations, the Reynolds number of the simulated flow is much smaller than in clouds. For this reason, our calculation may underestimate the influence of very large fluctuations of the velocity gradients on the statistical properties of the orientation of the ellipsoids, and on the collision rate. These effects remain to be understood.

Geometrical technicalities make a detailed analytical calculation of the collision rate difficult, thus preventing an accurate estimate in the case where particles follow the flow, as done in the case of droplets [50]. Simple estimates, however, can provide satisfactory predictions for the collision kernel, both in the presence and in the absence of gravitational settling, at least when the response time of the particles is sufficiently small compared to the smallest characteristic time in the flow, the Kolmogorov time. As already known for droplets, we find an important enhancement of the collision kernel for ellipsoids when particle relaxation time becomes large compared to the Kolmogorov time scale.

A first natural extension of the work would be to determine, under various assumptions concerning the collision (elastic, inelastic), the distribution of orientations and velocity statistics after collision. A second one would consist in considering the full four-way coupling (fluid \leftrightarrow particle \leftrightarrow particle) influence, and in particular how it affects the coagulation process, beyond the ghost-collision approximation. Investigating such processes requires more sophisticated numerical methods [54,55].

ACKNOWLEDGMENTS

We are thankful to S. Borrmann, K. Gustavsson, S. Malinowski, B. Mehlig, R. Shaw, and C. Siewert for discussions at various stages of the work. The simulations have been performed by using the local HPC facilities at ENS de Lyon (PSMN) and at the University Lyon-I (P2CHPD) mainly supported by the Auvergne-Rhône-Alpes region (Grant No. CPRT07-13 CIRA) and the project Equip@Meso (ANR-10-EQPX-29-01). A.N., E.L., and A.P. have been supported by the grant “TEC” 2 from A.N.R. (ANR-12-BS09-0011-02) and by the EU COST action MP0806 “Particles in Turbulence.” J.J. and A.P. acknowledge support from the Alexander von Humboldt-Stiftung.

-
- [1] H. R. Pruppacher and J. D. Klett, *Microphysics of Clouds and Precipitations* (Springer, Dordrecht, 2010).
 - [2] R. A. Shaw, Particle-turbulence interactions in atmospheric clouds, *Ann. Rev. Fluid Mech.* **35**, 183 (2003).
 - [3] E. Bodenschatz, S. P. Malinowski, R. A. Shaw, and F. Stratmann, Can we understand clouds without turbulence? *Science* **327**, 970 (2010).
 - [4] W. W. Grabowski and L. P. Wang, Growth of cloud droplets in a turbulent environment, *Ann. Rev. Fluid Mech.* **45**, 293 (2013).
 - [5] J. P. Chen and D. Lamb, The theoretical basis for the parameterization of ice crystal habits: Growth by vapor deposition, *J. Atmos. Sci.* **51**, 1206 (1994).
 - [6] T. Hashino, K. Y. Cheng, C. C. Chueh, and P. K. Wang, Numerical study of motion and stability of falling columnar crystals, *J. Atmos. Sci.* **73**, 1923 (2016).
 - [7] F. Yang, M. Ovchinnikov, and R. A. Shaw, Minimalist model of ice microphysics in mixed-phase stratiform clouds, *Geophys. Res. Lett.* **40**, 3756 (2013).
 - [8] F. Yang, M. Ovchinnikov, and R. A. Shaw, Microphysical consequences of the spatial distribution of ice nucleation in mixed-phase stratiform clouds, *Geophys. Res. Lett.* **41**, 5280 (2014).

- [9] G. A. Voth and A. Soldati, Anisotropic particles in turbulence, *Ann. Rev. Fluid Mech.* **49**, 249 (2017).
- [10] C. Siewert, R. P. J. Kunnen, and W. Schröder, Orientation statistics and settling velocity of ellipsoids in decaying turbulence, *Atmos. Res.* **142**, 45 (2014).
- [11] D. Lopez and E. Guazzelli, Inertial effects on fibers settling in a vortical flow, *Phys. Rev. Fluids* **2**, 024306 (2017).
- [12] K. Gustavsson, J. Jucha, A. Naso, E. Lévêque, A. Pumir, and B. Mehlig, Statistical Model for the Orientation of Nonspherical Particles Settling in Turbulence, *Phys. Rev. Lett.* **119**, 254501 (2017).
- [13] P. Yang, H. Wei, H.-L. Huang, B. A. Baum, Y. X. Hu, G. W. Kattawar, M. I. Mischenko, and Q. Fu, Scattering and absorption property database for nonspherical ice particles in the near-through far-infrared spectral region, *Appl. Opt.* **44**, 5512 (2005).
- [14] J. Um, G. M. McFarquhar, Y. P. Hong, S.-S. Lee, C. H. Jung, R. P. Lawson, and Q. Mo, Dimensions and aspect ratios of natural ice crystals, *Atmos. Chem. Phys.* **15**, 3933 (2015).
- [15] C. Siewert, R. P. J. Kunnen, and W. Schröder, Collision rates of small ellipsoids settling in turbulence, *J. Fluid Mech.* **758**, 686 (2014).
- [16] S. Sundaram and L. R. Collins, Collision statistics in an isotropic particle-laden turbulent suspension. Part 1. Direct numerical simulations, *J. Fluid Mech.* **335**, 75 (1997).
- [17] L. P. Wang, A. S. Wexler, and Y. Zhou, On the collision rate of small particles in isotropic turbulence. I. Zero inertia case, *Phys. Fluids* **10**, 266 (1998).
- [18] G. Falkovich, A. Fouxon, and M. G. Stepanov, Acceleration of rain initiation by cloud turbulence, *Nature (London)* **419**, 151 (2002).
- [19] M. Wilkinson and B. Mehlig, Caustics in turbulent aerosols, *Eur. Phys. Lett.* **71**, 186 (2005).
- [20] A. Pumir and M. Wilkinson, Collisional aggregation due to turbulence, *Ann. Rev. Condens. Matter Phys.* **7**, 141 (2016).
- [21] G. B. Jeffery, The motion of ellipsoid particles immersed in a viscous fluid, *Proc. Roy. Soc. A* **102**, 161 (1922).
- [22] J. Happel and H. Brenner, *Low Reynolds Number Hydrodynamics* (Martinus Nijhoff, The Hague, the Netherlands, 1983).
- [23] D. Donzis, P. K. Yeung, and K. R. Sreenivasan, Dissipation and enstrophy in isotropic turbulence: Resolution effects and direct numerical simulations, *Phys. Fluids* **20**, 045108 (2008).
- [24] S. A. Orszag, On the elimination of aliasing in finite-difference schemes by filtering high-wavenumber components, *J. Atmos. Sci.* **28**, 1074 (1971).
- [25] S. Elghobashi, On predicting particle-laden turbulent flows, *Appl. Sci. Res.* **52**, 309 (1994).
- [26] W. Grabowski and P. Vaillancourt, Comments on “preferential concentration of cloud droplets by turbulence: Effects on the early evolution of cumulus cloud droplet spectra,” *J. Atmos. Sci.* **56**, 1433 (1999).
- [27] L. P. Wang, O. Ayala, S. E. Kasprzak, and W. W. Grabowski, Theoretical formulation of collision rate and collision efficiency of hydrodynamically interacting cloud droplets in turbulent atmosphere, *J. Atmos. Sci.* **62**, 2433 (2005).
- [28] G. K. Batchelor and J. T. Green, Hydrodynamic interaction of two small freely-moving spheres in a linear flow field, *J. Fluid Mech.* **56**, 375 (1972).
- [29] J. Chun and D. L. Koch, Coagulation of monodisperse aerosol particles by isotropic turbulence, *Phys. Fluids* **17**, 027102 (2005).
- [30] K. Gustavsson, B. Mehlig, and M. Wilkinson, Collisions of particles advected in random flows, *New J. Phys.* **10**, 075014 (2008).
- [31] M. Voßkuhle, E. Lévêque, M. Wilkinson, and A. Pumir, Multiple collisions in turbulent flows, *Phys. Rev. E* **88**, 063008 (2013).
- [32] C. Siewert, R. P. J. Kunnen, M. Meinke, and W. Schröder, On the Collision Detection for Ellipsoidal Particles in Turbulence, in *Proceedings of the ASME 2014 4th Joint US-European Fluids Engineering Division Summer Meeting* (Chicago, Illinois, ASME, 2014), paper FEDS2014-2198.
- [33] Y. K. Choi, J. W. Chang, W. Wang, M.-S. Kim, and G. Elber, Continuous collision for ellipsoids, *IEEE Trans. Vis. Comput. Graphics* **15**, 311 (2009).

- [34] M. Voßkuhle, A. Pumir, E. Lévêque, and M. Wilkinson, Prevalence of the sling effect for enhancing collision rates in turbulent suspensions, *J. Fluid Mech.* **749**, 841 (2014).
- [35] R. G. Cox, The steady motion of particles of arbitrary shape at small Reynolds numbers, *J. Fluid Mech.* **23**, 625 (1965).
- [36] W. Chester, A general theory for the motion of a body through a fluid at low Reynolds number, *Proc. R. Soc. Lond. A* **430**, 89 (1990).
- [37] L. G. Leal, Particle motions in a viscous fluid, *Ann. Rev. Fluid Mech.* **12**, 435 (1980).
- [38] F. Candelier, J. Einarsson, and B. Mehlig, Angular Dynamics of a Small Particle in Turbulence, *Phys. Rev. Lett.* **117**, 204501 (2016).
- [39] J. D. Klett, Orientation model for particles in turbulence, *J. Atmos. Sci.* **52**, 2276 (1995).
- [40] K. M. Markowicz and M. L. Witek, Simulations of contrail optical properties and radiative forcing for various crystal shapes, *J. Appl. Meteor. Climatol.* **50**, 1740 (2011).
- [41] P. Yang, K. N. Liou, L. Bin, B. Yi, and B. A. Baum, On the radiative properties of ice clouds: Light scattering, remote sensing and radiation parametrization, *Adv. Atmos. Sci.* **32**, 32 (2015).
- [42] K. Gustavsson and B. Mehlig, Statistical models for spatial patterns of heavy particles in turbulence, *Adv. Phys.* **65**, 1 (2016).
- [43] M. Shin and D. L. Koch, Rotational and translational dispersion of fibers in isotropic turbulent flows, *J. Fluid Mech.* **540**, 143 (2005).
- [44] A. Pumir and M. Wilkinson, Orientation statistics of small particles in turbulence, *New J. Phys.* **13**, 093030 (2011).
- [45] S. Parsa, E. Calzavarini, F. Toschi, and G. A. Voth, Rotation Rate of Rods in Turbulent Fluid Flows, *Phys. Rev. Lett.* **109**, 134501 (2012).
- [46] L. Chevillard and C. Meneveau, Orientation dynamics of small, triaxial-ellipsoidal particles in isotropic turbulence, *J. Fluid Mech.* **737**, 571 (2013).
- [47] K. Gustavsson, J. Einarsson, and B. Mehlig, Tumbling of Small Axisymmetric Particles in Random and Turbulent Flows, *Phys. Rev. Lett.* **112**, 014501 (2014).
- [48] G. H. Good, P. J. Ireland, G. P. Bewley, E. Bodenschatz, L. R. Collins, and Z. Warhaft, Settling regimes of inertial particles in isotropic turbulence, *J. Fluid Mech.* **759**, R3 (2014).
- [49] M. Gibert, H. Xu, and E. Bodenschatz, Where do small weakly inertial particles go in a turbulent flow? *J. Fluid Mech.* **698**, 160 (2012).
- [50] P. G. Saffman and J. S. Turner, On the collision of droplets in turbulent clouds, *J. Fluid Mech.* **1**, 16 (1956).
- [51] G. Falkovich and A. Pumir, Sling effect in collisions of water droplets in turbulent clouds, *J. Atmos. Sci.* **64**, 4497 (2007).
- [52] O. Ayala, B. Rosa, L. P. Wang, and W. W. Grabowski, Effects of turbulence on the geometric collision rate of sedimenting droplets. Part 1. Results from direct numerical simulation, *New J. Phys.* **10**, 075015 (2008).
- [53] O. Ayala, B. Rosa, and L. P. Wang, Effects of turbulence on the geometric collision rate of sedimenting droplets. Part 2. Theory and parameterization, *New J. Phys.* **10**, 075016 (2008).
- [54] S. Tao, Z. Guo, and L.-P. Wang, Numerical study on the sedimentation of single and multiple slippery particles in a Newtonian fluid, *Powder Tech.* **315**, 126 (2017).
- [55] N. Geneva, C. Peng, X. Li, and L.-P. Wang, A scalable interface-resolved simulation of particle-laden flow using the lattice Boltzmann method, *Parallel Comput.* **67**, 20 (2017).